On the Numerical Dispersion of the Radial Point Interpolation Meshless (RPIM) Method in Lossy Media

Xiaoyan Zhang [1,2], Zhizhang (David) Chen [3*], and Yiqiang Yu [1,3]

[1] School of Information Engineering
East China Jiaotong University, Nanchang, 330013,China

[2] State Key Laboratory of Millimeter Waves, Nanjin, 210096, China
xy_zhang3129@ecjtu.jx.cn

[3] Department of Electrical and Computer Engineering
Dalhousie University, NS B3J 2X4, Canada
*zz.chen@ieee.org, yiqiang.yu@dal.ca

Abstract ─ A general formula for numerical dispersion of the two-dimensional time-domain radial point interpolation meshless (2-D RPIM) method is analytically derived. Numerical loss and dispersion characteristics of the RPIM method with both Gaussian and multiquadric basis functions are investigated. It is found that numerical loss and dispersion errors of the RPIM vary with types of basis functions used and associated parameters, number of the nodes, and medium conductivities. In addition, condition numbers of the moment matrix of the meshless methods can also increase numerical dispersion errors. With a reasonable condition number of the moment matrix, the radial point interpolation meshless methods perform generally better than the FDTD method in terms of numerical dispersion errors.

Index Terms ─ Gaussian basis function, multiquadric basis function, numerical dispersion, radial point interpolation method (RPIM).

I. INTRODUCTION

Meshless or mesh-free methods present alternative methods to replace the mesh/grid based methods for electromagnetic field modeling. Time-domain radial point interpolation meshless (RPIM) method is one of the typical meshless methods. References [1, 2] show that it may be equivalent to the finite-difference time-domain (FDTD) method under certain conditions. But in a general case, it promises better accuracy and computational efficiency in solving the problems of irregular or multiscale structures [3, 4]. The numerical results show that the RPIM approach can reduce about 80% of the number of unknowns and about 70% of the computational time in comparison with the FDTD method. The RPIM can not only save more than 60% of the memory required by the FDTD method, but also run 100% faster.

Recently, the RPIM method was successfully applied to solve various electromagnetic problems. Rodrigo *et al*. proposed an improved Lennard-Jones discretization method for the RPIM and validated it with a scattering problem [5]. Tanaka *et al.* investigated a unique meshless method using the RPIM and applied it to an eddy current problem [6]. Khalef combined a Crank–Nicolson scheme with the RPIM and utilized it to model waveguide problems [7]. However, when radial basis functions (RBFs) and interpolating points are not properly chosen for solving Maxwell's equations, the meshless methods can become erroneous and even divergent, which limits further engineering applications of the RPIM [8, 9]. Therefore, it is important to investigate errors of the meshless methods. One of the errors of main concerns is numerical dispersion of a meshless method.

In 2008, Lai *et al.* derived a numerical dispersion relationship for the RPIM method in lossless media [10], but it is only for one-dimensional structure and the dispersion characteristics of the RPIM method have not been well studied. In 2013, Ansarizadeh and Movahhedi investigated dispersion error of the RPIM method by tracing the propagation of the electromagnetic wave [11]. Their work also focused on the lossless media and they did not derive a general formula for the numerical dispersion of the RPIM method. In 2014, we studied the numerical dispersion of the RPIM method and its relationship to the finite-difference time-domain (FDTD) approach [1], but it is only for the Gaussian basis function with two adjacent points in lossless media. In 2017, we derived a general formula for numerical dispersion of the RPIM method in lossless media [12]. Since then, no more numerical dispersion analysis of the RPIM method has been reported. Important issues such as node density, other non-Gaussian basis functions [6,

Submitted On: June 12, 2018
Accepted On: October 25, 2018

13] and their impacts on numerical dispersions in lossy media have not been studied.

In this paper, we address the above issues: we first develop the general numerical dispersion relation of the RPIM method for both lossless and lossy medium, verify it with the FDTD method when its node distributions are made to be the same as that of the FDTD, and then investigate numerical dispersion properties of the RPIM method with different basis functions, number of nodes and conductivities. To our best knowledge, these issues have not been reported in the past.

It is worth to mention here that the meshless method is expected to have smaller numerical dispersion errors than the conventional FDTD method; this is because the meshless methods use high-order basis functions to expand the fields than the roof-top basis functions used in the FDTD method [14]. Our investigations presented here show that it is true in general but not so under certain conditions because of the meshless methods involve more complex matrix operations.

II. NUMERICAL DISPERSION FORMULATION

For simplicity, a two-dimensional (2-D) TM_z wave propagating in a lossy and isotropic source-free medium of permittivity ε, conductivity σ, and permeability μ is considered. Maxwell's equations in time domain can be written in a matrix form as:

$$\begin{bmatrix} \varepsilon\frac{\partial}{\partial t}+\sigma & \frac{\partial}{\partial y} & -\frac{\partial}{\partial x} \\ \frac{\partial}{\partial y} & \mu\frac{\partial}{\partial t} & 0 \\ \frac{\partial}{\partial x} & 0 & -\mu\frac{\partial}{\partial t} \end{bmatrix} \begin{bmatrix} E_z \\ H_x \\ H_y \end{bmatrix} = 0 . \quad (1)$$

Take E_z for an inspection. As Fig. 1 shows, E_z at node k can be interpolated with field values at the neighboring nodes j that is within the support domain centered at node k. Its node-based expansion can be expressed as [3]:

$$E_z(X_k) = \sum_{j=1}^{N} \Psi_j(X_k) \cdot E_z(X_j) = \boldsymbol{\Psi}(X_k)\boldsymbol{E}_z(\boldsymbol{X}_j), \quad (2)$$

where $X_k = (x_k, y_k)$ represents spatial position of node k, $\boldsymbol{X}_j = (X_1, X_2, \cdots, X_N)$ stores all the node locations, and N is the total number of nodes within the support domain. Then, vector $\boldsymbol{\Psi}(X_k) = [\Psi_1(X_k), \Psi_2(X_k), \cdots \Psi_N(X_k)]$ is a shape function, which is determined by:

$$\boldsymbol{\Psi}(\mathrm{X}_k) = \boldsymbol{r}(\mathrm{X}_k)^T \boldsymbol{G}^{-1}. \quad (3)$$

Here $\boldsymbol{r}(\mathrm{X}_k) = [r_1(\mathrm{X}_k), r_2(\mathrm{X}_k), \cdots r_N(\mathrm{X}_k)]$ is a basis function. For Gaussian function, $r_j(\mathrm{X}_k)$ has the following form [3, 4]:

$$r_j(X_k) = \exp(-\alpha_c \frac{|X_j - X_k|^2}{d_c^2}), \quad (4)$$

where α_c is the shape parameter, d_c is the minimum distance between two nodes. For a multi-quadric basis function with shape parameters of C and q, $r_j(\mathrm{X}_k)$ has the following form [6]:

$$r_j(X_k) = \left(\frac{|X_j - X_k|^2}{d_c^2} + C^2 \right)^q . \quad (5)$$

Then, the moment matrix $\boldsymbol{G}$ in (3) is:

$$\boldsymbol{G} = \begin{bmatrix} 1 & r_2(X_1) & \cdots & r_N(X_1) \\ r_1(X_2) & 1 & \cdots & r_N(X_2) \\ \vdots & \vdots & \ddots & \vdots \\ r_1(X_N) & r_2(X_N) & \cdots & 1 \end{bmatrix}. \quad (6)$$

Let X_E and X_H denote the spatial positions of the nodes at which electric field and magnetic field are located, respectively. By substituting these formulas into (1), we can get:

$$\varepsilon\frac{\partial \boldsymbol{E}_z(X_E)}{\partial t} + \sigma \boldsymbol{E}_z(X_E) = -\boldsymbol{\Psi}'_y(X_E)\boldsymbol{H}_x(X_H) + \boldsymbol{\Psi}'_x(X_E)\boldsymbol{H}_y(X_H), \quad (7a)$$

$$\frac{\partial \boldsymbol{H}_x(X_H)}{\partial t} = -\frac{1}{\mu}\boldsymbol{\Psi}'_y(X_H)\boldsymbol{E}_z(X_E), \quad (7b)$$

$$\frac{\partial \boldsymbol{H}_y(X_H)}{\partial t} = \frac{1}{\mu}\boldsymbol{\Psi}'_x(X_H)\boldsymbol{E}_z(X_E). \quad (7c)$$

Here $\boldsymbol{\Psi}'_\xi = \partial\boldsymbol{\Psi}/\partial\xi$ ($\xi = x, y, z$).

By following the Fourier analysis approach [15], the numerical dispersion relation can be obtained. That is, first, the field components in (7) are assumed to have the following form:

$$f(\boldsymbol{r}, t) = f_0 \exp(-j\boldsymbol{k}\cdot\boldsymbol{r})\exp(j\omega t), \quad (8)$$

where ω is angular frequency, f_0 is the amplitude. $\boldsymbol{k} = k_x\mathbf{a}_x + k_y\mathbf{a}_y = (\beta + j\alpha)(\mathbf{a}_x\cos\phi + \mathbf{a}_y\sin\phi)$, with β being the phase shift constant, α being the attenuation constant and ϕ being the propagation angle with respect the x-axis. $\boldsymbol{r}$ is the displacement vector.

We then apply the time-average (TA) scheme [16] to the lossy term of (7a) and use the central finite-difference to approximate the time derivatives. Then, substitution of (8) into (7) reads:

$$E_{z0}e^{-j\boldsymbol{k}\cdot\boldsymbol{r}_E}\boldsymbol{\varphi}_1\boldsymbol{\varphi}_t = \boldsymbol{\Phi}(X_E)\begin{bmatrix} H_{x0} \\ H_{y0} \end{bmatrix} e^{-j\boldsymbol{k}\cdot\boldsymbol{r}_H}, \quad (9a)$$

$$H_{x0}e^{-j\boldsymbol{k}\cdot\boldsymbol{r}_H}\boldsymbol{\varphi}_2\boldsymbol{\varphi}_t = -\frac{1}{\mu}\boldsymbol{\Psi}'_y(X_H)E_{z0}e^{-j\boldsymbol{k}\cdot\boldsymbol{r}_E}, \quad (9b)$$

$$H_{y0}e^{-j\boldsymbol{k}\cdot\boldsymbol{r}_H}\boldsymbol{\varphi}_2\boldsymbol{\varphi}_t = \frac{1}{\mu}\boldsymbol{\Psi}'_x(X_H)E_{z0}e^{-j\boldsymbol{k}\cdot\boldsymbol{r}_E}. \quad (9c)$$

Here Δt is the time step and is set as $d_c / 2v_0$ to be consistent with FDTD method. v_0 is the speed of light. $\boldsymbol{\varphi}_1$, $\boldsymbol{\varphi}_2$, $\boldsymbol{\varphi}_t$, and $\boldsymbol{\Phi}(X_E)$ are defined as:

$$\boldsymbol{\varphi}_1 = \begin{bmatrix} 1 & 1 \\ -1 & 1 \end{bmatrix} \begin{bmatrix} \varepsilon / \Delta t \\ \sigma / 2 \end{bmatrix}, \boldsymbol{\varphi}_2 = \begin{bmatrix} 1 & -1 \end{bmatrix}, \boldsymbol{\varphi}_t = \begin{bmatrix} e^{j\omega\Delta t/2} \\ e^{-j\omega\Delta t/2} \end{bmatrix}, \quad (10)$$

$$\boldsymbol{\Phi}(X_E) = \begin{bmatrix} -\boldsymbol{\Psi}'_y(X_E) & \boldsymbol{\Psi}'_x(X_E) \end{bmatrix}. \quad (11)$$

After some manipulations, the following equations are obtained:

$$\begin{bmatrix} \varepsilon^{TA} c_0 & \boldsymbol{\Psi}'_y(X_E)\boldsymbol{Q}_E & -\boldsymbol{\Psi}'_x(X_E)\boldsymbol{Q}_E \\ \dfrac{\boldsymbol{\Psi}'_y(X_H)\boldsymbol{Q}_H}{\mu c_0} & 1 & 0 \\ -\dfrac{\boldsymbol{\Psi}'_x(X_H)\boldsymbol{Q}_H}{\mu c_0} & 0 & 1 \end{bmatrix} \begin{bmatrix} E_{z0} \\ H_{x0} \\ H_{y0} \end{bmatrix} = 0, \quad (12)$$

with

$$\boldsymbol{Q}_E = \left[e^{-j\boldsymbol{k}\cdot\Delta\boldsymbol{r}_1^E}, e^{-j\boldsymbol{k}\cdot\Delta\boldsymbol{r}_2^E}, \cdots, e^{-j\boldsymbol{k}\cdot\Delta\boldsymbol{r}_N^E} \right]^T, \quad (13a)$$

$$\boldsymbol{Q}_H = \left[e^{-j\boldsymbol{k}\cdot\Delta\boldsymbol{r}_1^H}, e^{-j\boldsymbol{k}\cdot\Delta\boldsymbol{r}_2^H}, \cdots, e^{-j\boldsymbol{k}\cdot\Delta\boldsymbol{r}_N^H} \right]^T. \quad (13b)$$

Here, $\Delta\boldsymbol{r}_j^E = \boldsymbol{r}_j^H - \boldsymbol{r}^E$, $\Delta\boldsymbol{r}_j^H = \boldsymbol{r}_j^E - \boldsymbol{r}^H$, $\boldsymbol{r}^H$ and $\boldsymbol{r}^E$ are the displacement vectors of magnetic field and electric field respectively. $c_0 = 2j\sin\theta_t / \Delta t$, $i = \sqrt{-1}$ and $\theta_t = \omega\Delta t / 2$. $\varepsilon^{TA} = \varepsilon - j\sigma\Delta t / 2\tan\theta_t$.

By setting the determinant of the coefficient matrix of (12) to zero, and with some manipulations, numerical dispersion relation can be obtained as:

$$\varepsilon^{TA}\mu c_0^2 = \boldsymbol{\Psi}'_y(X_E)(\boldsymbol{\Psi}'_y(X_H)\boldsymbol{Q}_H)\boldsymbol{Q}_E + \boldsymbol{\Psi}'_x(X_E)(\boldsymbol{\Psi}'_x(X_H)\boldsymbol{Q}_H)\boldsymbol{Q}_E. \quad (14)$$

This equation is solved with Newton iteration method.

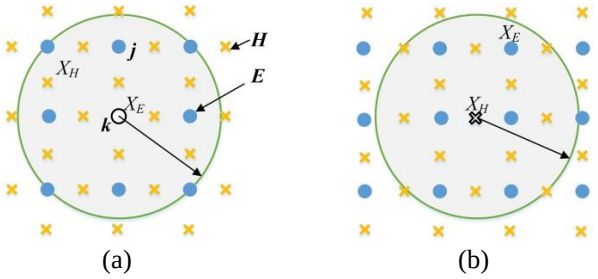

(a) (b)

Fig. 1. The support domain centered at node *k* and used in formulas (7a) (a) and of (7b) and (7c) (b).

III. DISPERSION ANALYSIS OF THE MESHLESS METHODS

In the following paragraphs, we conduct numerical dispersion analysis of the meshless methods. To do so, we define numerical loss error (*NLE*), numerical phase error (*NPE*) as follows [17]:

$$NLE = \left| \frac{\alpha_{num} - \alpha_0}{\alpha_0} \right| \times 100\%, \quad (15a)$$

$$NPE = \left| \frac{\beta_{num} - \beta_0}{\beta_0} \right| \times 100\%. \quad (15b)$$

β_{num} and α_{num} are the phase shift and attenuation constants of the meshless methods computed with (14), respectively. β_0 and α_0 are the theoretical phase shift and attenuation constants, respectively. With the above definitions, the dispersion errors of the meshless methods are studied as follows.

A. Effects of basis functions and their parameters

First, *N* is set to 4 and the distance between adjacent nodes is $\Delta s = \lambda/20$. Such a setting is comparable to the conventional finite-difference time-domain (FDTD) method where a field component at a grid point is related to the field components at the surrounding four grid points. The dielectric constant of the medium under consideration is $\varepsilon_r = 1$ and the conductivity is $\sigma = 0.001$ S/m.

Figure 2 shows the *NLE*s and *NPE*s of the RPIM and the FDTD methods. The RPIM method uses Gaussian basis function with different α_c values. It can be seen that when $\alpha_c = 10^{-4}$, the dispersion errors of the RPIM method are almost the same as those of the FDTD method, which is consistent with the phenomenon described in [1]; when $\alpha_c = 10^{-3}$, the *NLE*s and *NPE*s of the RPIM method are both less than the errors of the FDTD method; however, when $\alpha_c = 10^{-2}$, their *NLE*s and *NPE*s are sharply increased. This means that using a large α_c will result in a large error or even solution divergence.

Figure 3 shows the condition number of the moment matrix $\boldsymbol{G}$ in (6) versus different α_c. As α_c decreases, the condition number of $\boldsymbol{G}$ increases rapidly. It implies that $\boldsymbol{G}$ can become an ill-conditioned matrix and unstable solutions are more likely to occur with a small α_c. In other words, choosing a smaller α_c does not necessarily lead to smaller errors because of potential large condition numbers of the moment matrix. To ensure both the stability and accuracy of the RPIM method, we select α_c at the range of 10^{-3} in the following studies.

We now turn to the RPIM method with the multiquadric basis function of (5). First, we set the parameter q=0.01 and let C change from 0.3 to 10. Figure 4 shows the numerical dispersion errors with changing C. Then, we let the value of q change with a fixed C=1. Figure 5 shows the numerical dispersion errors with changing q.

From Fig. 4 (a), we can see that the *NLE*s of the

RPIM method with the multiquadric basis function are approximately equal to or less than those of FDTD method in most of the propagation angles. With small *C*, however, the *NPE*s can be larger than those of FDTD approach at some propagation angles (see Fig. 4 (b)).

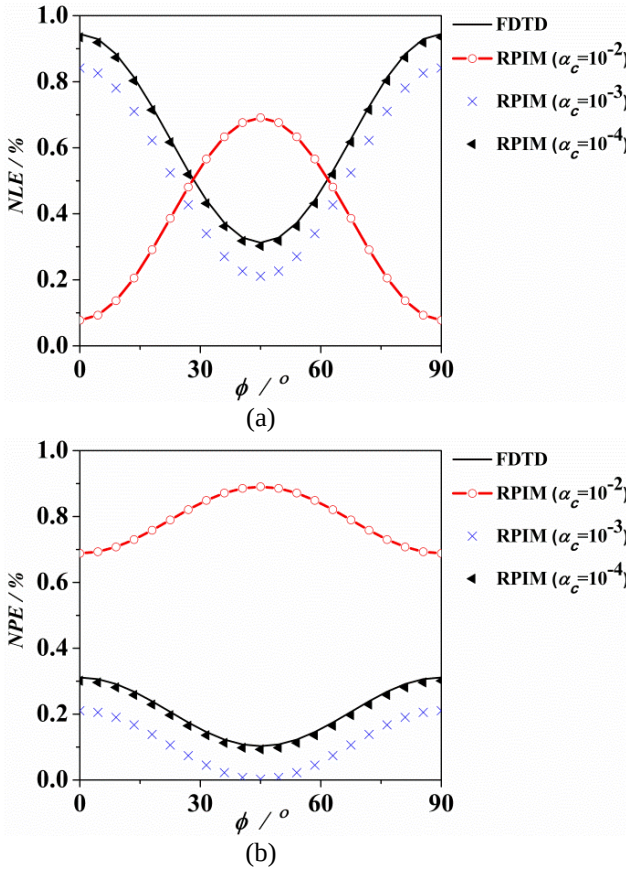

Fig. 2. Numerical dispersion of the RPIM method: (a) *NLE* and (b) *NPE* versus the angle of propagation in a medium of ε_r=1 and σ=0.001S/m.

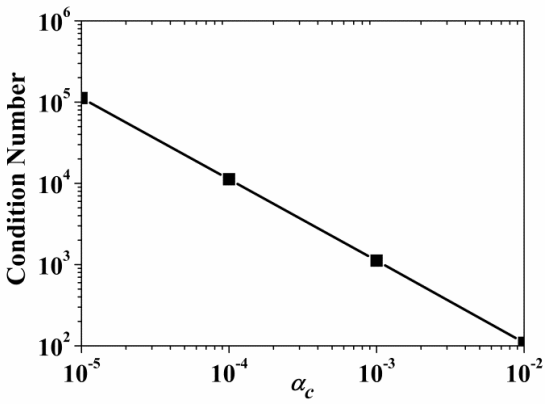

Fig. 3. Condition number of the moment matrix *G* versus different α_c of Gaussian basis function.

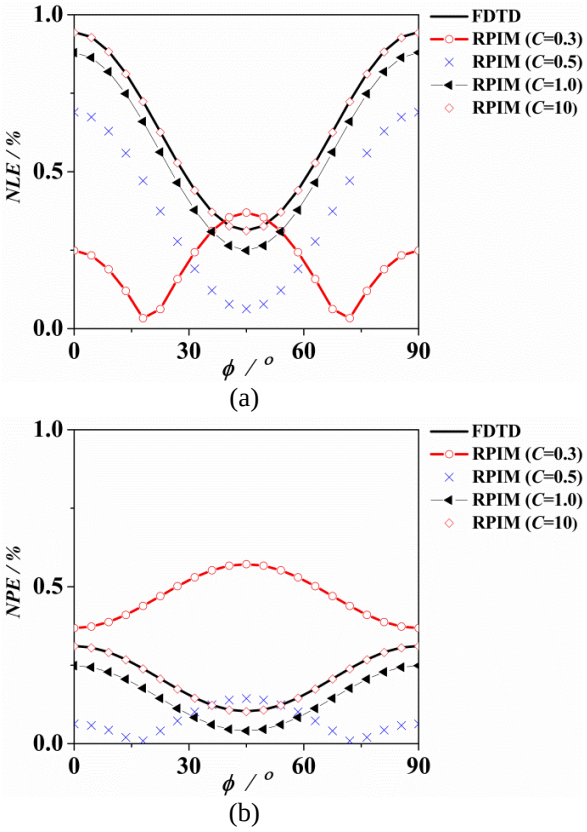

Fig. 4. Numerical dispersion of the RPIM method using the multiquadric basis function: (a) *NLE* and (b) *NPE* of the RPIM method versus the angle of propagation. *q*=0.01. *C* is changed from 0.3 to 10. *N*=4 and σ=0.001 S/m.

From Fig. 5, we can see that *q* has little effect on the *NLE*s and *NPE*s of the algorithm. Therefore, numerical dispersion errors of the RPIM method with the multiquadric basis function are mainly determined by *C*.

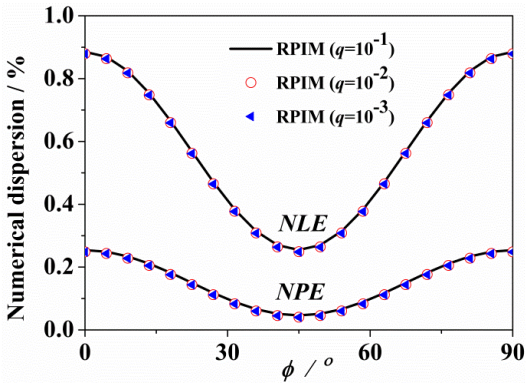

Fig. 5. Numerical dispersion of the RPIM method using the multiquadric basis function of the RPIM method versus the angle of propagation with *q*=0.01, 0.01 and 0.001, respectively. In all cases, *C*=1, *N*=4, and σ=0.001 S/m.

Figure 6 gives the condition numbers of the moment matrix ***G*** versus different *C*. Comparing Fig. 6 with Fig. 3, we can clearly see that the condition numbers of ***G*** based on multiquadric function are far greater than that of ***G*** with Gaussian function; in other words, when the RPIM uses the multiquadric function as basis function, its coefficient matrix is more prone to be system singularity or numerical instability than that with Gaussian basis function.

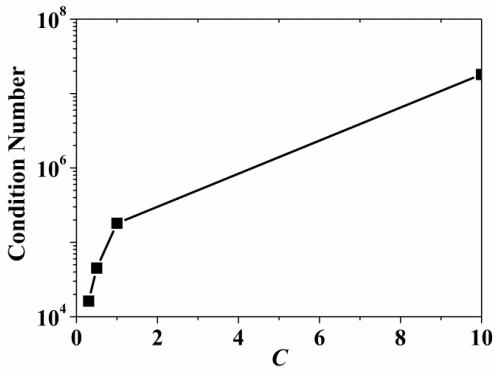

Fig. 6. Condition number of the moment matrix *G* versus different *C* of multiquadric basis function.

Hence, based on the above analyses, in balancing between the modeling accuracy and the matrix condition number, it can be concluded that Gaussian basis function is a better choice for the RPIM approach for electromagnetic modeling. Therefore, in the following investigation, we use Gaussian basis function.

B. Effects of numbers of the nodes within a support domain

In this subsection, we investigate the effect of the number *N* of the nodes within a support domain. This is an important study as the results may provide a practical guideline on how to choose the number of nodes that can provide the best accuracy with least possible computational expenditure. The numbers of the node points are *N*=4, 12(α_c =0.001) and 16(α_c =0.003, for solution stability), respectively, with the change of the size of the support domain. The conductivity of the medium is σ=0.1 S/m.

Figure 7 shows the numerical dispersions. As seen, when *N*=4, the numerical dispersion errors approximately equal to those of the FDTD method; when *N*=12, the *NLE*s and the *NPE*s of the algorithm are also less than the errors of the FDTD approach; however, when *N*=16, although the *NPE*s of the meshless method are smaller than those of the FDTD method, almost all of the *NLE*s are far greater than them. The reason is that the condition number of ***G*** is significantly increased when *N*=16 (see Fig. 8). Although we can increase the value of α_c to reduce the condition number of the moment matrix, only the *NPE*s of the algorithm will decrease but not necessarily *NLE*. Clearly, the *NLE* is more sensitive than the *NPE* to the singularity of the moment matrix. In weighting all the above factors, we conclude that only when the moment matrix becomes nonsingular, numerical dispersion errors of the RPIM method can be reduced by increasing the number of the nodes.

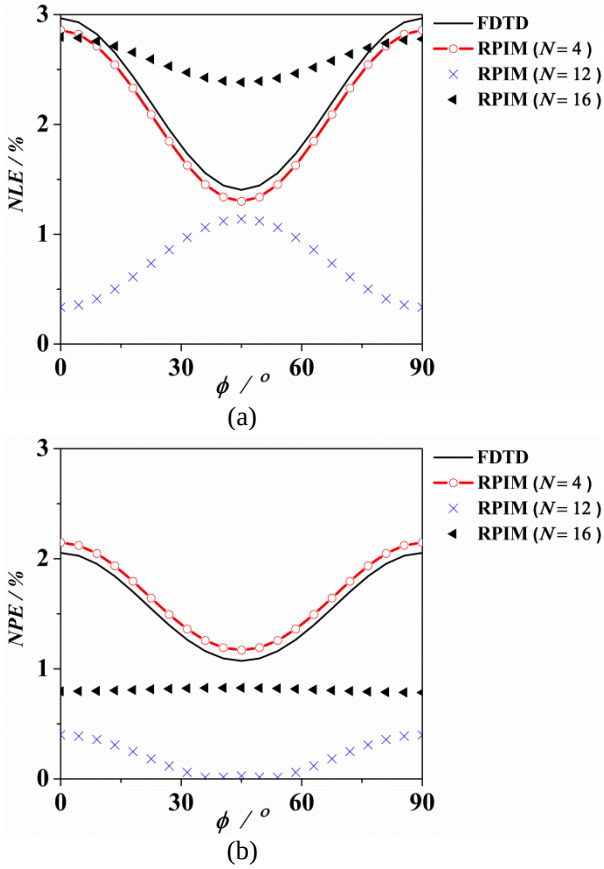

Fig. 7. Numerical dispersion of the RPIM method with Gaussian basis function: (a) *NLE* and (b) *NPE* versus *N*. $\Delta s=\lambda/20$ and σ=0.1 S/m.

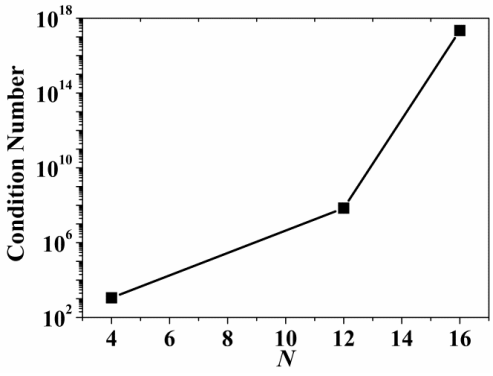

Fig. 8. Condition number of the moment matrix *G* versus different *N*.

C. Effects of media's conductivity

In this subsection, we investigate the effect of conductivity of the medium. σ=0.001 S/m, 0.1 S/m, and 1 S/m are used as the conductivity of the medium under consideration, respectively. For obtaining a stable solution, N is set to 4 with α_c =0.001.

Figure 9 shows the *NLE*s and *NPE*s of the RPIM method. The *NLE*s and the *NPE*s of the method increase with the increase of σ. And the increase of the *NPE*s is much larger than that of the *NLE*s. Therefore, the electromagnetic wave propagation in lossy dielectric may lead to greater numerical dispersion error than in free space.

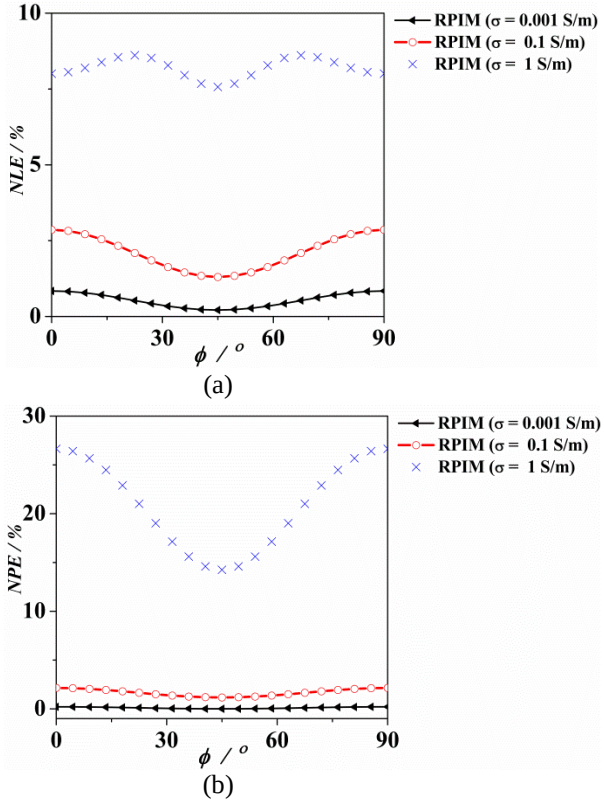

Fig. 9. Numerical dispersion of the RPIM method with Gaussian basis function: (a) *NLE* and (b) *NPE* versus conductivity. N=4, $\Delta s=\lambda/20$, and $\alpha_c = 0.001$.

IV. CONCLUSION

The general relation for numerical dispersion of the RPIM method is derived and analyzed for both lossless and lossy media in this paper. It was shown that only when the moment matrix is nonsingular, the numerical dispersion error of the RPIM can be less than that of the FDTD method. Solution stability and accuracy of the RPIM method are also influenced by the types of the basis functions and the number of nodes. The moment matrix of the RPIM with multiquadric basis function is more prone to be ill-conditioned than Gaussian function. Moreover, the *NLE* of the meshless method is more sensitive than the *NPE* to the singularity of the moment matrix; therefore, the balances between the solution stability (as a result of the ill-condition) and solution accuracy should be considered when choosing the modeling parameters. Another finding is that increase of medium conductivity leads to increase of numerical dispersion error.

Finally, it is noted that the FDTD method can be considered as a special case of the meshless methods with low-order roof-top functions as the basis functions [14], [18], [19], [20]. As a result, the meshless methods are expected to have smaller numerical errors in general but not always due to the conditions and complexity of the moment matrix. This is shown in this paper.

ACKNOWLEDGMENT

The authors wish to acknowledge the supports of National Natural Science Foundation of China through Grant #61471107, #61761017, Open Project of State Key Laboratory of Millimeter Waves through Grant #K201829 and the Natural Science and Engineering Research Council (NSERC) of Canada through its discovery program.

REFERENCES

[1] S. Yang, Z. Chen, Y. Yu, and S. Ponomarenko, "On the numerical dispersion of the radial point interpolation meshless method," *IEEE Microwave And Wireless Components Letters*, vol. 24, no. 10, pp. 653-655, Oct. 2014.

[2] T. Kaufmann, C. Fumeaux, and R. Vahldieck, "The meshless radial point interpolation method for time-domain electromagnetics," *2008 IEEE MTT-S International Microwave Symposium Digest*, Atlanta, USA, pp. 61-64, Sep. 2008.

[3] Y. Yu, F. Jolani, and Z. Chen, "An efficient meshless approach to multi-scale modeling in the time-domain," *The Applied Computational Electromagnetics Society*, vol. 27, no. 6, pp. 466-474, June 2012.

[4] Y. Yu and Z. Chen, "A 3-D radial point interpolation method for meshless time-domain modeling," *IEEE Transactions on Microwave Theory and Techniques*, vol. 57, no. 8, pp. 2015-2020, Aug. 2009.

[5] R. M. S. de Oliveira, W. C. B. Sousa, and W. R. M. Rabelo, "A meshless discretization methodology based on lennard-jones forces," *IEEE Antennas and Wireless Propagation Letters*, vol. 16, pp. 1492-1495, June 2017.

[6] Y. Tanaka, S. Watanabe, and T. Oko, "Study of eddy current analysis by a meshless method using RPIM," *IEEE Transactions on Magnetics*, vol. 51, no. 3, pp. 7201404, Mar. 2015.

[7] R. Khalef, M. T. Benhabiles, F. Grine, and M. L.

Riabi, "An unconditionally stable radial point interpolation meshless method based on the Crank–Nicolson scheme solution of wave equation," *IEEE Transactions on Microwave Theory and Techniques*, vol. 66, no. 8, pp. 3705-3713, Aug. 2018.

[8] T. Kaufmann, C. Engström, C. Fumeaux, and R. Vahldieck, "Eigenvalue analysis and longtime stability of resonant structures for the meshless radial point interpolation method in time domain," *IEEE Transactions on Microwave Theory and Techniques*, vol. 58, no. 12, pp. 3399-3408, Dec. 2010.

[9] Y. Zhang, K. R. Shao, Y. Guo, J. Zhu, D. X. Xie, and J. D. Lavers, "A comparison of point interpolative boundary meshless method based on PBF and RBF for transient eddy-current analysis," *IEEE Transactions on Magnetics*, vol. 43, no. 4, pp. 1497-1500, Apr. 2007.

[10] S. J. Lai, B. Z. Wang, and Y. Duan, "Meshless radial basis function method for transient electromagnetic computations," *IEEE Trans. Magnetics*, vol. 44, no. 10, pp. 2288-2295, Oct. 2008.

[11] F. Ansarizadeh and M. Movahhedi, "Unconditionally-stable meshless methods using different split-step techniques and their phase velocity considerations," *The Applied Computational Electromagnetics Society*, vol. 28, no. 9, pp. 788-794, Sep. 2013.

[12] X. Zhang, P. Ye, Z. Chen, and Y. Yu, "Numerical dispersion analysis of radial point interpolation meshless method," *2017 Progress in Electromagnetics Research Symposium*, Singapore, pp. 717-719, Nov. 2015.

[13] Z. Shaterian, T. Kaufmann, and C. Fumeaux, "On the choice of basis functions for the meshless radial point interpolation method with small local support domains," *IEEE International Conference on Computational Electromagnetics*, Hong Kong, China, pp. 288-290, Feb. 2015.

[14] Z. Chen and S. Luo, "Generalization of the finite-difference-based time-domain methods using the method of moments," *IEEE Transactions on Microwave Theory and Techniques*, vol. 54, no. 9, pp. 2515-2524, Sep. 2006.

[15] G. Sun and C. W. Trueman, "Numerical dispersion and numerical loss in explicit finite-difference time-domain methods in lossy media," *IEEE Transactions on Antennas and Propagation*, vol. 53, no. 11, pp. 3684-3690, Nov. 2005.

[16] J. A. Pereda, O. García, A. Vegas, and A. Prieto, "Numerical dispersion and stability analysis of the FDTD technique in lossy dielectrics," *IEEE Microwave and Guided Wave Letters*, vol. 8, no. 7, pp. 245-247, July 1998.

[17] G. Sun, X. Ma, and Z. Bai, "Numerical stability and dispersion analysis of the precise-integration time-domain method in lossy media," *IEEE Transactions on Microwave Theory and Techniques*, vol. 60, no. 9, pp. 2723-2729, Sep. 2012.

[18] Z. Chen and M. Ney, "Method of weighted residuals: a general approach to deriving time- and frequency-domain numerical methods," *IEEE Antennas and Propagation Magazines*, vol. 51, no. 1, pp. 51-70, Feb. 2009.

[19] Z. Chen, "How can we unify numerical methods with a single mathematic framework?," *Proceedings of 2014 Asia-Pacific Conference on Antennas and Propagation*, Harbin, China, pp. 1392-1395, July 2014.

[20] J. Wang, Z. Chen, J. Li, Y. Yu, and J. Liang, "Towards a unifying computational platform with the node-based meshless method," *Proceedings of 2018 IEEE International Microwave Symposium*, Pennsylvania, USA, pp. 1017-1020, June 2018.

Xianyan Zhang received the B.S. degree in Applied Physics and M.S. degree in Physical Electronics from Yunnan University, Kunming, China, in 2001 and 2004 respectively, and the Ph.D. degree in Electromagnetic Field and Microwave Technology from Institute of Electronics, Chinese Academy of Sciences in 2007.

Her research interests include electromagnetic computation, antenna design and wireless power transmission structure design.

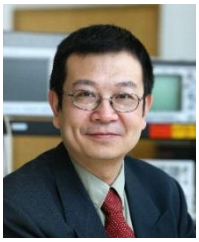

Zhizhang (David) Chen received the bachelor's degree from Fuzhou University, the Master degree in Radio Engineering from Southeast University, P. R. China, the Ph.D. degree in Electrical Engineering from the University of Ottawa, Canada. He was a NSERC Post-doctoral Fellow with McGill University, Montreal, Canada. He is currently a Professor with Dalhousie University, Halifax, Nova Scotia, Canada, where he has served as the Head of the Department of Electrical and Computer Engineering. He has been an Adjunct or Visiting Professor with the University of Nottingham of UK, École Nationale Supérieure des Télécommunications de Bretagne of France, Shanghai Jiaotong University,

Beihang University, Fuzhou University and the University of Electronic Science and Technology of China.

Chen has authored and coauthored over 350 journal and conference papers in computational electromagnetics, RF/microwave electronics, antennas, and wireless technologies. His current research interests are in time-domain electromagnetic modeling techniques, ultra-wideband wireless communication systems and wireless power transfer technology. He received the 2005 Nova Scotia Engineering Award, a 2006 Dalhousie Graduate Teaching Award, the 2007 & 2015 Dalhousie Faculty of Engineering Research Award and the 2013 IEEE Canada Fessenden Medal. He is the Fellow of the IEEE, the Canadian Academy of Engineering and the Engineering Institute of Canada.

Yiqiang Yu received the M.S. degree in Communication Systems in 2003 and the Ph.D. in Microwave Communications Engineering in 2007 from Swansea University, U.K.

He is an Associate Professor with East China Jiaotong University. He is also an Adjunct Professor with the University of Electronic Science and Technology of China and Dalhousie University, Halifax, Canada. He is also the CEO of Chengdu Sprouting Technology Co. Ltd. His primary interest is in applications of computational electromagnetics. His interests also include wireless power transmission structure design, antennas design and measurement, EMI/EMC analysis and testing.